Separation Characteristics of Swirl-Tube Dust Separators

Weiming Peng and Alex C. Hoffmann
Dept. of Physics, University of Bergen, Allegt 55, 5007 Bergen, Norway

Huub Dries
Shell Global Solutions Int., 1030 BN Amsterdam, The Netherlands

Experimental results for the overall efficiency, pressure drop, and grade efficiency curves (GECs) in a laboratory cylindrical swirl tube with inlet vanes are given and compared with experimental data and model predictions for a tangential-inlet, cylinder-on-cone cyclone, tested in the same rig. The results show that the performance of swirl tubes is comparable with that of cyclones in spite of the simpler body shape, and also that swirl tubes are more compact than cyclones when operating at the same pressure drop and capacity and with the same cut point (efficiency). The S shape of the GEC in swirl tubes, however, differs in steepness from that of conventional cyclones. That steepness m (larger m, steeper GEC, that is, sharper cut) had values between 2.5 and 3 in the swirl tube and around 4 in the cyclone. The values found for the swirl tube are still well within the range of 2–4 often seen in industrial cyclones. The swirl tube GEC, while less steep around the 50% mark, is steeper at larger particle sizes. Using Stokesian scaling, the GECs from the laboratory swirl tube, which was working alone, are also compared with experimental GECs from a commercial swirl-tube installation, in which the swirl tubes work in parallel. The commercial GEC is found to be slightly less steep: this, in fact, favors the separation of "microfines" (responsible for equipment fouling), while the separation of coarse particles remains sufficiently large. Underperformance of the commercial installation due to cross talk could not be detected. © 2004 American Institute of Chemical Engineers *AIChE J,* 50: 87–96, 2004

Keywords: gas cleaning, cyclone, swirl tube, separation efficiency, pressure drop, grade-efficiency curve

Introduction

Centrifugal separators spin a gas stream to remove entrained particles by centrifugal action without moving parts. They play a dominating role in dedusting and demisting in industry. They are easy and inexpensive to make, relatively economical to operate, and adaptable to a wide range of operating conditions. Efficient, reliable separation is needed to meet ever more stringent environmental legislation. Using improved cyclone technology to meet these new emission limits is better in terms of process operation and process economics than using more expensive and cumbersome dedusting alternatives.

While conventional cyclones have a cylinder-on-cone shape, and often a tangential inlet, as shown in the lefthand side of Figure 1, centrifugal separators can also be purely cylindrical, as seen in the righthand side. Such a shape is often combined with an axial gas inlet with swirl vanes, and is here referred to as a "swirl tube." Swirl tubes have distinct advantages over cylinder-on-cone separators in that the body is much easier to construct and has high mechanical integrity, a significant ad-

Correspondence concerning this article should be addressed to A. C. Hoffmann at alex.hoffmann@fi.uib.no.

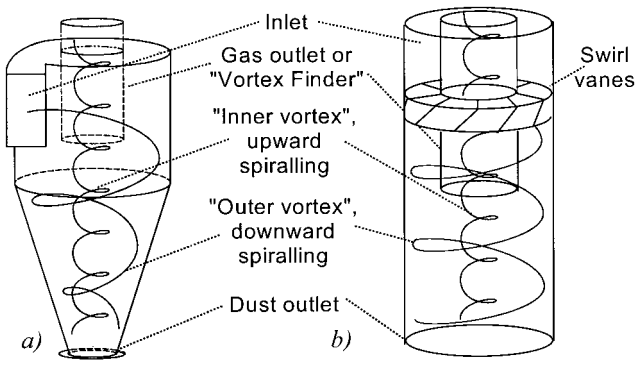

Figure 1. (a) A cylinder-on-cone cyclone with a tangential inlet, and (b) a cylindrical swirl tube with swirl vanes, and with the flow pattern indicated.

vantage when the separators are to work under harsh conditions, possibly equipped with a refractory lining, such as in the FCC process. Furthermore swirl tubes are even less prone to clogging than normal cyclones, and very "forgiving" for changes in the operating conditions.

The swirl vanes give rise to a strongly swirling flow that centrifuges the particles to the wall along which they are transported to the solids outlet. In a reverse-flow swirl tube, the vanes are arranged around the gas outlet, or vortex finder. The gas swirls downward in the outer part of the separation space, and the particles are centrifuged out to the wall. The gas reverses its axial flow direction as it moves inwards and spins upwards in the central part, exiting through the vortex finder. The particles leave the swirl tube through the bottom, which may or may not be equipped with a base plate leaving an annular gap through which the particles flow.

Swirl tubes are often used in final-stage, high-efficiency dedusters operating at moderate or low solids loadings. The tubes are mostly arranged in parallel with a large number of smaller tubes in "swirl decks" (see Figure 2), in which they are fed from—and discharge to—common plenums. Contrary to conventional cyclones, a small gas stream is often drawn from the dust plenum of the swirl deck, the so-called underflow. This flow has to be dealt with downstream. Upstream of the swirl deck, large-diameter conventional cyclones are often installed as a first dedusting step that collects the particles directly without requiring an underflow stream and is economical both in terms of investment and running costs.

Swirl tubes are used for the cleaning of industrial gases, the separation of catalyst from reactive gases or the cleaning of exhaust gases before power recovery systems. In addition to compactness, advantages of swirl tubes are often called "lower pressure drop" and "higher capacity," although the basis for comparison is often not clear. Another often quoted advantage is "more stable flow." One of the objects of this article is to clarify these issues.

Conventional cylinder-on-cone cyclones with tangential inlets are the subject of a large number of research articles, in which they have been studied experimentally and numerically. Their grade-efficiency curves (GECs) have been determined by experiment, and their flow pattern has been measured, for instance, using laser Doppler anemometry (LDA) and simulated by computational fluid dynamics (CFD). Much less attention has been paid to the flow pattern and the GECs in swirl tubes.

For this article to be self-contained we briefly review the relevant basic issues, while referring to Hoffmann and Stein (2002) for a general introduction to gas cyclone technology.

The separation performance of centrifugal separators under different operating conditions needs to be compared by a measure that is independent of the feed particle-size distribution. The overall efficiency, η_T, is therefore not suitable, but the grade efficiency—the separation efficiency for one particular particle size, $\eta(x)$—is, since it only depends on the feed density (and not even on that, if the particle size is reported as the so-called aerodynamic particle size).

The basic equations for calculating the grade efficiency $\eta(x)$ from the particle-size distributions are (Svarovsky, 1984; Hoffmann and Stein, 2002)

$$\eta(x) = \eta_T \frac{dF_c(x)}{dF(x)} = 1 - (1 - \eta_T) \frac{dF_f(x)}{dF(x)}; \qquad \frac{1}{\eta(x)} = 1 + \left(\frac{1}{\eta_T} - 1\right) \frac{dF_f(x)}{dF_c(x)} \quad (1)$$

where $F_c(x)$, $F_f(x)$, and $F(x)$ are the cumulative (volumetric) size distributions of the captured, the lost (or "fine"), and the feed material fractions, respectively.

The GEC, $\eta(x)$, usually has an S shape, as shown in Figure 3. Once the GEC is known for a given set of operating conditions, the total efficiency for a particular feed-size distribution can be computed by integration

$$\eta_T = \int_0^1 \eta(x)\, dF_f. \quad (2)$$

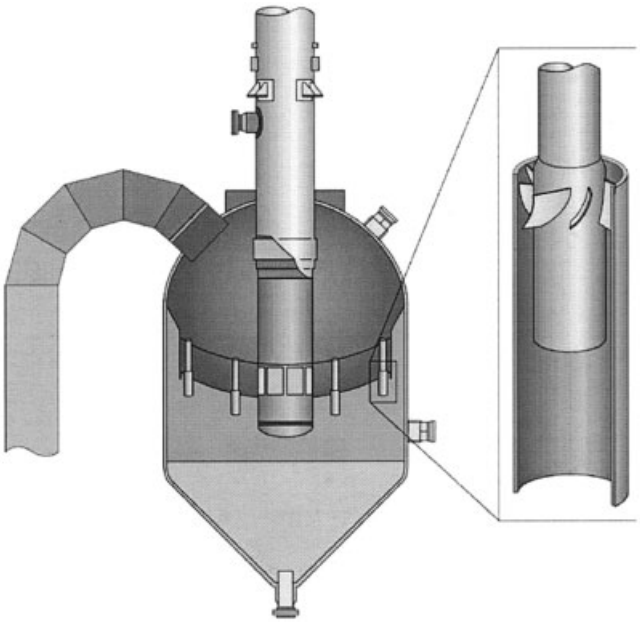

Figure 2. The Shell TSS with a swirl tube (Dries and Patel, 2000).

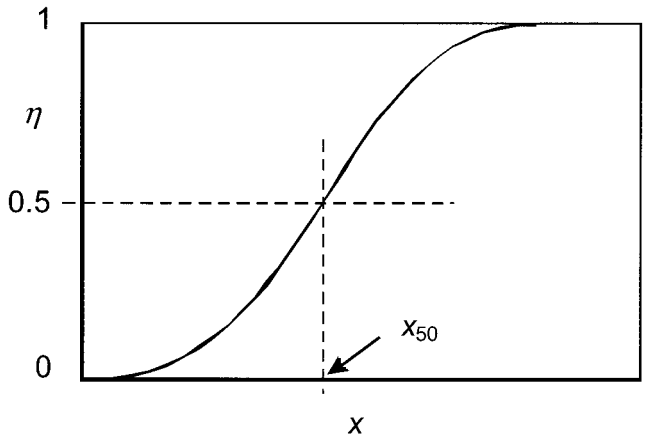

Figure 3. Typical GEC with the cut-size, x_{50} indicated. GEC's tend to be similarly shaped when plotted against ln(x). The function (4), which is fitted to the experimental GEC's here, has a slope of $m/4$ at the cut-size when plotted against ln(x).

The shape of the GEC strongly depends on the particle motion in the separators, which again depends on the operational conditions and the geometrical design. Note that the GEC is pushed upward (better separation for all particle sizes) if the solids loading is elevated, and that if an elevated solids loading influences the separation significantly, Eq. 2 only remains valid if the GEC is determined at the proper solids loading. In this study the solids loading was kept low.

Rather than generating the entire GEC, the separation performance from experiments under different operational conditions can be compared using the so-called cut size, x_{50}, which is defined as the particle size with 50% probability of being separated (also indicated in Figure 3). Obviously, if the shape of the GEC is similar, the smaller the value of the cut size, the higher the overall separation efficiency.

The slope of the GEC indicates the "sharpness of cut." There are many ways to represent this, for example (Svarovsky, 1984)

$$H_{25/75} = \frac{x_{25}}{x_{75}} \tag{3}$$

Another way is to fit a functional form to the GEC. One is (for example, Hoffmann and Stein, 2002)

$$\eta(x) = \frac{1}{1 + \left(\frac{x_{50}}{x}\right)^m} \tag{4}$$

where the exponent m is a measure of the steepness of the GEC (sharpness of cut). The larger m is, the steeper the curve, and for infinite m the GEC approaches a stair-step shape, indicating that the separator is collecting all particles greater than the cut point and losing those that are smaller. Dirgo and Leith (1985) found m to be 6.4 when fitting Eq. 4 to Barth's (1956) standard GEC, which was based on experimental data for tangential-entry cyclones and given in graphical form. In many commercial cyclones, the value of m is somewhat lower, often falling within the range between 2 and 4.

The efficiency of centrifugal separators can be predicted by CFD simulations. This is mostly done by Lagrangian particle tracking in a precalculated flow field. CFD can be very helpful for detailed investigation of the flow in the separator and the separation of individual size-classes of particles. Many uncertainties remain, however, in calculating both the flow field and the efficiency by particle tracking. These uncertainties are perhaps not given sufficient exposure in the literature. 3-Dimensional (3-D) rather than 2-D modeling is the trend; although the work of Hoekstra et al. (1999) shows that there is not a great deal of difference between the two, even for cyclones with a tangential inlet. The most promising CFD approach today seems to be large-eddy simulation (LES), where the larger eddies are simulated directly and the smaller, subgrid eddies are modeled by a turbulence model.

Analytical models used to predict the separation performance can be divided into two main groups. The first class, the most popular modeling approach (Barth, 1956; Dietz, 1968; Trefz, 1992; Mothes and Löffler, 1988; Clift et al., 1991), is the "equilibrium-orbit" model, based on a force balance on a particle swirling on the interface between the "inner" and "outer" vortex. Barth's original simple expression for the cut size is

$$x_{50} = \sqrt{\frac{v_{rCS} 9 \mu D_x}{\rho_p v_{\theta CS}^2}}, \tag{5}$$

where v_{rCS} and $v_{\theta CS}$ are the radial and tangential velocities in the surface CS, created by elongating the vortex-finder wall to the bottom of the cyclone, μ is the gas viscosity, D_x is the vortex-finder diameter, and ρ_p is the particle density. The other class of model originated in the work of Rosin (1932), and is often referred to as the time-of-flight type of model. It considers whether a particle injected into the cyclone at a certain radial position and spiraling downwards has sufficient time to reach the cyclone wall before reaching the bottom. The particle cut size is given by Rosin as

$$x_{50} = \sqrt{\frac{9 b \mu}{\pi N_s v_{in} (\rho_p - \rho)}}, \tag{6}$$

where b is the inlet width, N_s is the number of spiral turns the particle takes on its way toward the bottom of the cyclone, v_{in} is the inlet velocity, and ρ is the gas density. The Rietema (1959) model, based on the same concept, gives the following expression for x_{50}

$$C_{y50} \frac{x_{50}^2 (\rho_p - \rho)}{\mu} H \frac{\Delta p}{pQ} = 3.5 \tag{7}$$

where Δp is the cyclone pressure drop, Q is the volumetric gas flow rate, H is the total height of the cyclone, and C_{y50} is a "characteristic cyclone number" determined empirically. We note that the analysis of Rietema assumes that the separator has a conical shape.

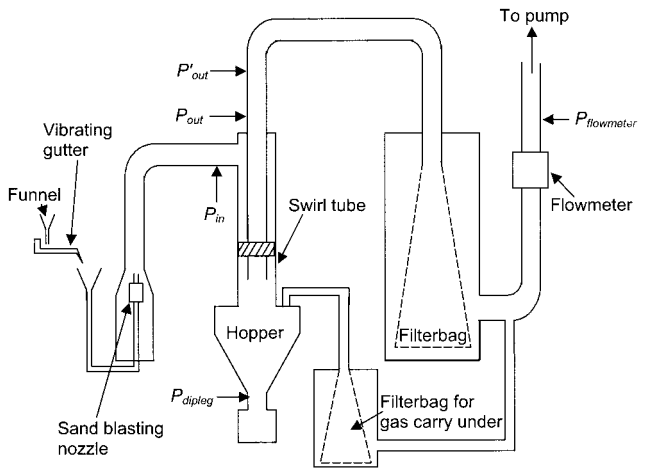

Figure 4. Setup for the separation performance test in swirl tubes.

These models, and most of the literature on centrifugal separators, are concerned with traditional tangential-entry, cylinder-on-cone cyclones. This work was undertaken to study the working of swirl tubes, and compare their performance with that of traditional cyclones.

Experiments

Test rig

The experimental setup is shown in Figure 4. The gas flow is generated by a Siemens vacuum roots blower that draws the solids-laden gas through the system. By using a sandblasting nozzle the solids are homogeneously dispersed in the gas flow on the cyclone inlet side. A bleed flow marked "gas carry under" can be taken from the top of the powder collection chamber marked "hopper" through a small filter, as indicated in the figure. This bleed flow simulates industrial conditions in swirl-tube separators, where a 3% "carryunder" helps in carrying the catalyst out of the swirl tubes.

The system is based on total capture of the lost fraction in the membrane-coated Goretex filter bag after the cyclone. This filterbag can be weighed *in situ.* The separation efficiency can thus be determined, and the mass balance checked, by weighing the mass of solids in all three streams: charged, collected, and lost. Since the filter provides barrier filtration, the powder can be removed after weighing for size analysis to determine the grade-efficiency curve.

The swirl tube model used was made from Perspex, and care was taken to avoid problems arising from accumulation of static electrical charge during the tests. More details about the experimental setup are given in earlier articles (for example, Hoffmann et al., 2001).

Experimental program

During each experiment, the pressure drop was monitored and after the experiment the overall efficiency was determined. The lost and collected solids fractions were collected and reduced in size using a spinning riffler for particle-size analysis in a Joyce-Loebl centrifuge. Some of the experiments were repeats to ascertain the reproducibility of the results.

The swirl tube is shown in Figure 5; the dimensions are given in mm. The value of L_2 was varied, taking on 5 different values: 240, 295, 350, 405, and 460 mm.

The experimental conditions were approximately:

- Solids loading: 1.6 g solids/m^3 gas;
- Volumetric gas flow: $Q = 0.103$ m^3/s for all tests except one where $Q = 0.089$ m^3/s.

The test dust used was a chalk powder with a particle density of 2730 kg/m^3. The size distribution of the powder is well fitted by a log-normal distribution with mean -12.52 and a spread of 1.0; thus, the median particle size is 3.65 μm.

Results

The overall efficiency and the pressure drop are plotted in Figures 6 and 7. These and other tests show that increasing the dimensionless length L_2/D increase the separation efficiency and decrease the pressure drop. This is in line with earlier findings for traditional cyclones (Hoffmann et al., 2001).

Swirl-tube GECs from two repeat experiments are given in Figure 8, where the general shape and the degree of reproducibility are shown. One notices straight away that the shape deviates from the typical S shape seen in conventional cylinder-on-cone, tangential-inlet cyclones.

Figure 9 shows the effect of the inlet flow rate on the GEC. As expected, a decrease in the inlet flow leads (through a decrease in the swirl velocity) to deterioration in the separation efficiency, translating the GEC to the right. This is, in part,

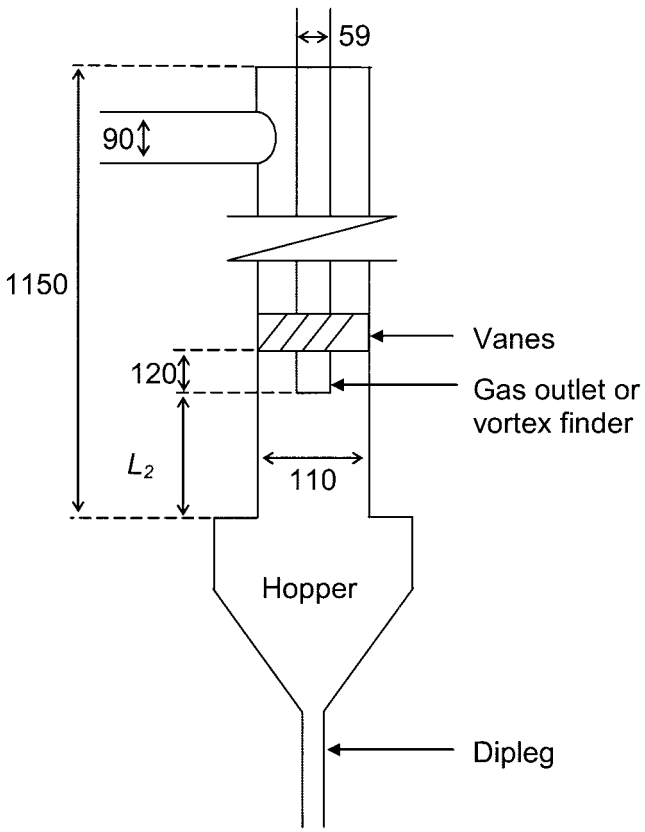

Figure 5. The swirl tube; the dimensions are given in mm.

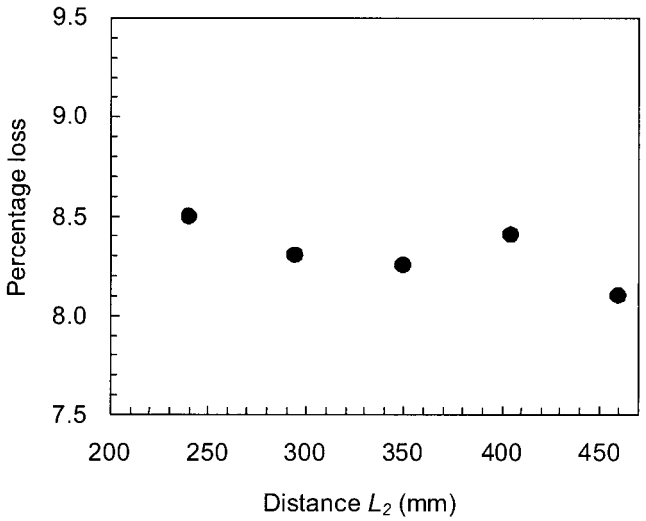

Figure 6. Effect of the length L_2 on the separation efficiency.

counteracted by the difference in length: the swirl tube with the lower flow is longer, which tends to make it more efficient.

Discussion

Comparison of experimental cut sizes with model predictions

So far, there is no convincing evidence that one particular CFD technique has proven globally more successful for modeling different types of cyclones than are the model approaches mentioned earlier in this article.

Most cyclone models are geared to tangential inlet cyclones. While a satisfactory dedicated swirl-tube model is not yet available, it is possible to apply these cyclone models to swirl tubes by calculating an equivalent "inlet velocity" in the swirl tubes. This can be done in the following way.

The swirl velocity is assumed to be uniform over the cross section in the gas just emanating from the vane pack

$$v_{\theta av} = \frac{Q}{F \tan\theta} = \frac{Q}{\pi(R_w^2 - R_o^2)\tan\theta} \tag{8}$$

where F the horizontal cross-sectional area of the vanes' outlet section, θ is the exit angle of the vanes with the horizontal, and R_w and R_o the inner radius of the cyclone wall and the outer radius of the vortex finder, respectively. This simple formula assumes that the thickness of the vanes themselves does not restrict the area available for flow significantly. If it does, a more accurate expression can be found in Hoffmann and Stein (2002).

As the gas moves down from the vane pack, the vortex will rather quickly adjust so that the swirl velocity at an axial station further from the vane exit will have the distribution shown in Figure 10 and roughly described by

$$v_\theta = \frac{c}{r^n} \tag{9}$$

If there is negligible loss between the two stations, the total angular momentum should be the same

$$\sum\left(\frac{\rho}{2}(v_\theta r)r\Delta r\right)_1 = \sum r\left(\frac{\rho}{2}(v_\theta r)r\Delta r\right)_2 \tag{10}$$

Integrating Eq. 10, from R_o, the outside diameter of the vortex finder to R_w, the wall diameter of the swirl tube, and using Eq. 9 for v_θ at station 2, gives

$$c = \frac{3-n}{3\pi}\cdot Q \cdot \frac{R_w^3 - R_o^3}{(R_w^2 - R_o^2)(R_w^{3-n} - R_o^{3-n})\tan\theta} \tag{11}$$

The swirl velocity close to the wall of the swirl tube is therefore

$$v_{\theta w} = \frac{c}{R_w^n} = \frac{1}{R_w^n}\cdot\frac{3-n}{3\pi}\cdot Q \cdot \frac{R_w^3 - R_o^3}{(R_w^2 - R_o^2)(R_w^{3-n} - R_o^{3-n})\tan\theta} \tag{12}$$

As a rough estimate, this wall velocity can be taken as the "equivalent inlet velocity" to use in the cyclone models. It is well known that the wall velocity in tangential entry cyclones will be somewhat higher than the inlet velocity due to constriction of the inlet jet, and more precise relations can be formulated on the basis of published estimates of this acceleration. The inlet dimensions, if they are required for the model calculations (inlet height/inlet width $\cong$ 2), are then given by the "inlet velocity" and Q.

The predictions based on some of the cyclone models used in this way are compared with the experimental results in Figure 11. Since grade-efficiency curves were only available from a few experiments, the cut sizes were estimated from the overall separation efficiencies, assuming the separator to have a sharp cut

$$1 - \eta = F_f(x_{50}) \tag{13}$$

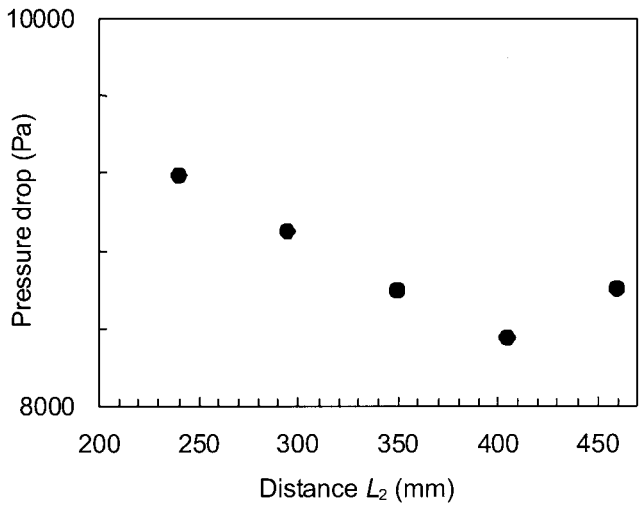

Figure 7. Effect of the length L_2 on the pressure drop.

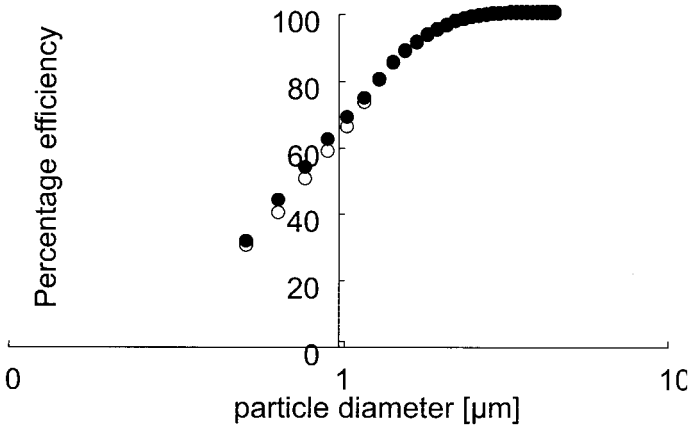

Figure 8. Experimental data showing the general shape of swirl-tube GEC curves and the degree of reproducibility of the results: Q = 0.097 and 0.099 m^3/s, respectively, for the two experiments, and L_2 is 240 mm.

The Rietema model agrees reasonably well with the experimental results. The other two models underpredict the separation performance of the swirl tube.

Comparison of the overall performance of the swirl tube and the cyclone

Svarovsky (1986) gives the following expression as a scaling rule for the performance of "well designed cyclones"

$$Eu\sqrt{Stk_{50}} = \sqrt{12} \tag{14}$$

$$Stk_{50} = \frac{\Delta\rho x_{50}^2 v_z}{18\mu D}; \qquad Eu = \frac{\Delta p}{\frac{1}{2}\rho v_z^2} \tag{15}$$

where v_z is the mean axial velocity in the separator body.

The results for the swirl tube and earlier results from a tangential-inlet, cylinder-on-cone cyclone generated in the same setup and under the same experimental conditions (Hoffmann et al., 2001) are compared with Eq. 14 in Figure 12.

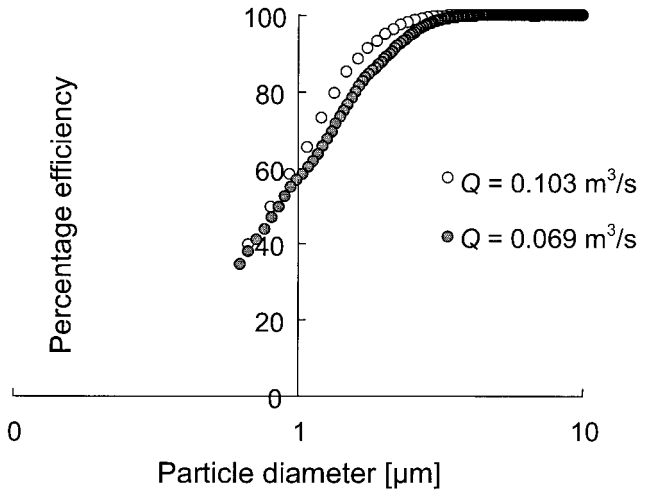

Figure 9. Effect of the volumetric flow rate on the GEC of a given swirl tube.

It is clearly seen that the results for the swirl tube fall close to the line representing Eq. 14, so that the swirl tube can be said to act as a "well designed cyclone." What makes the comparison between the cyclone and swirl tube in Figure 12 very relevant is that both devices were tested in the same experimental setup using the same experimental procedures and conditions and the same test dust.

By judicious use of the scaling laws and simple models for the pressure drop and the effect of changing D_x on the cut size, x_{50}, it is possible to use the present data to roughly compare swirl tubes and cyclones directly. Details of such calculations are available from the authors. For instance, we can estimate in the following way the pressure drop Δp of a cyclone having the same D, Q, and x_{50} as the swirl tube:

- From the experimental results in the cyclone, use Stokesian scaling (see the subsection titled "Comparison of the laboratory swirl-tube performance with a commercial TSS instillation" below) to find the cut size, x_{50}, in a geometrically similar cyclone with the same diameter D and the same flow rate Q as the swirl tube.
- Change the vortex finder diameter D_x in this cyclone until the x_{50} is the same as in the swirl tube, using simple models to estimate the effect of changing D_x on x_{50} and Δp.

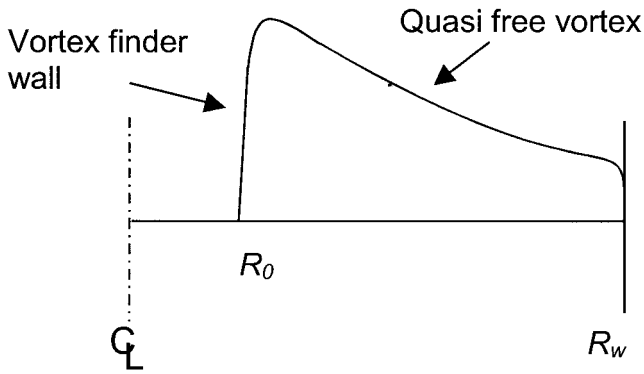

Figure 10. The tangential velocity profile between the vortex finder and the outer wall in cyclones and swirl tubes.

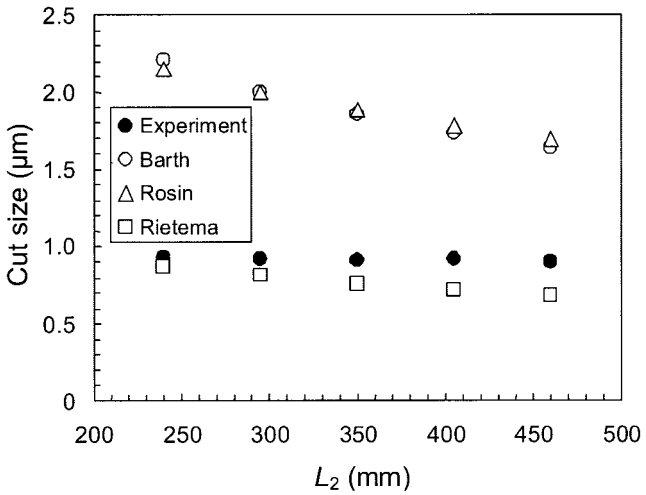

Figure 11. Comparison of the experimental results for the cut size with model predictions.

In this way we find that the pressure drop in a cyclone working with the same D, Q, and x_{50} will be some 80% higher than in the swirl tube. Similarly we can find that the diameter D of a cyclone working with the same Q, x_{50}, and Δp as the swirl tube will be some 30% higher than that of the swirl tube.

We thus confirm the claims made for swirl tubes mentioned in the introduction of "lower pressure drop" and "higher capacity" compared with conventional cyclones, at least for equipment of the basic designs we tested in our laboratory.

Comparison of the GECs in swirl tubes and cyclones

A GEC from the swirl tube with $L_2 = 350$ mm and $Q = 0.069$ m^3/s, is shown in Figure 13 together with one from our cyclone experiments (the cyclone body diameter D was 0.2 m, the solids loading was 2 g/m^3, and Q was 0.111 m^3/s).

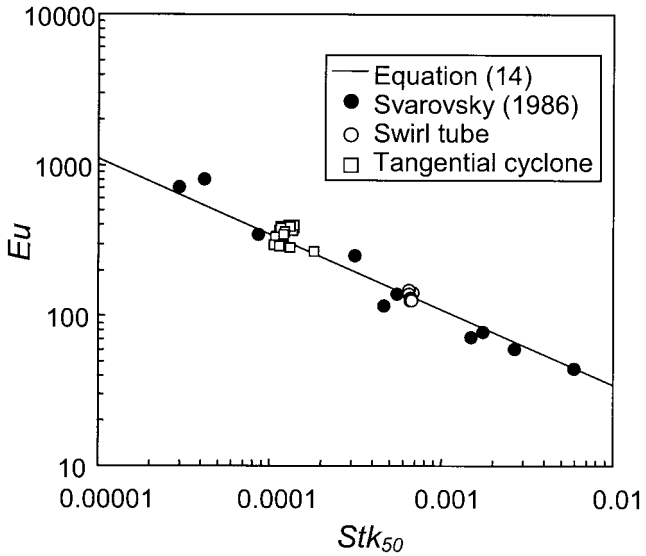

Figure 12. *Eu* versus Stk_{50}, showing experimental points from the cyclone and swirl tube together with the data and equation of Svarovsky.

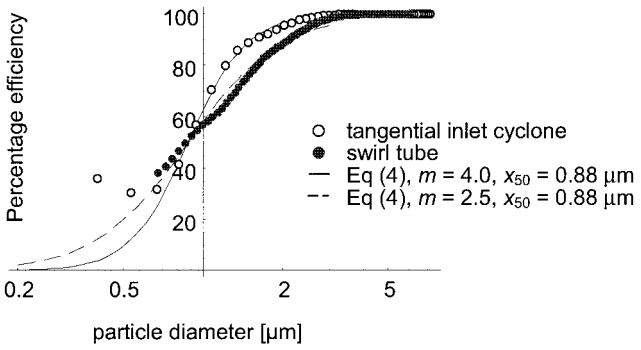

Figure 13. Grade efficiency data for the swirl tube (closed points) and the tangential inlet cyclone, both with fitted curves according to Eq. 4.

Since the size of the separators and the operating conditions were different, the object of this figure is not to compare their absolute performance, but to compare the shape of the GECs under conditions where the two separators happen to have the same cut size of 0.88 μm.

We see that the swirl tube and the tangential-inlet, cylinder-on-cone cyclone both have GECs of similar form. The GEC of the cyclone is, however, much steeper around the cut size. The "duck-tail" phenomenon, sometimes appearing in cyclones, is clearly seen in the cyclone GEC: a higher efficiency for small particles in the very fine range. This is not seen in the swirl-tube data, but these data are not sufficiently reliable in the fine end to make any definite statement about this.

If Eq. 4 is fitted to the swirl-tube GECs, we find the exponent m to lie between 2.5 and 3.0, and the curve in the figure is fitted by Eq. 4 with $m = 2.5$. Fitting Eq. 4 to the cyclone grade-efficiency data gives $m = 4.0$. Thus the value of m in the swirl tube is somewhat lower than that in the cyclone, but still well within the range of 2–4 found in conventional industrial cyclones. At larger particle sizes (around 2 μm), the swirl tube GEC is steeper than that of the conventional cyclone.

Comparison of the laboratory swirl-tube performance with a commercial TSS installation

The swirl-tube GECs shown earlier have been generated in a laboratory model working alone. It is valuable to compare the

Table 1. Physical Data for the Swirl-Tube Model and the Commercial Installation

	Model	Comm.
Body diameter (D)	0.110 m	0.247 m
Inside diameter of gas outlet (D_x)	0.059 m	0.140 m
Ratio of body to gas outlet diameter	0.54	0.57
Exit angle from vanes	30°	30°
Superficial axial velocity (v_z)	10.8 m/s	14.0 m/s
Density of gas (ρ)	1.2 kg/m^3	1.08 kg/m^3
Viscosity of gas (μ)	1.81×10^{-5} kg/m · s	3.85×10^{-5} kg/m s
Density of particles (ρ_p)	2730 kg/m^3	1600 kg/m^3
Mean size of particles (x_{mean})	3.6×10^{-6} m	15×10^{-6} m

results with a commercial swirl-tube installation operating under quite different circumstances.

In the "shell TSS," swirl tubes working in parallel separate catalyst particles from flue gases at elevated temperature and pressure. The swirl tubes are charged from, and discharge to, common plenums. The device is further described by Dries and Patel (2000), and shown in Figure 2.

The physical data pertaining to the laboratory model and the commercial installation are summarized in Table 1.

The comparison is done by predicting the performance of the commercial unit from that of the laboratory model by Stokesian scaling and comparing these predictions with experimental GECs from the commercial installation.

Stokesian scaling is based on the assumption that, if two separators with diameters D_a and D_b are geometrically similar, their separation efficiencies are similar, in the sense that particles having the same Stokes number Stk are captured with the same efficiency (Hoffmann and Stein, 2002). We define Stk_η as the Stokes number corresponding to a given efficiency η (where η is 50% for the cut size), neglecting the small gas density

$$Stk_\eta = \frac{\rho_p x_\eta^2 v_z}{18\mu D} \tag{16}$$

where x_η is the diameter of the particle captured with an efficiency of η. We can then write for two separators designated by subscripts a and b

$$Stk_\eta = \frac{\rho_{pa} x_{\eta a}^2 v_{za}}{18\mu_a D_a} = \frac{\rho_{pb} x_{\eta b}^2 v_{zb}}{18\mu_b D_b} = \text{const.} \tag{17}$$

With this formula the separation efficiency of the swirl tube in the commercial installation can be predicted from the experimental results in the laboratory swirl tube.

For this to be valid, the tubes must, as mentioned, be geometrically similar. In this context the exit angle from the swirl vanes and the size of the gas outlets, D_x, relative to the body diameter, D, are the most important geometrical parameters. They are seen in Table 1 to be the same between the two.

The efficiency of commercial third-stage separators is determined by sampling the flue gas at both inlet and outlet, measuring the concentration of dust, as well as the particle size of that dust [see Figures 14 and 15, also discussed in Dries and Patel (2000)]. The comparison between the scaled laboratory swirl-tube data and the commercial multi-swirl-tube assembly is seen in Figure 16. Obviously the scaled GEC from the laboratory model matches the commercial data well, particularly the data marked "Commercial 4/98."

One important factor that may influence the efficiency of multiple swirl tubes is cross talk, the possibility that imbalance occurs, resulting in gas flow from one swirl tube to the other through the plenums connecting them (e.g., Behrouzi, 1988). The agreement between predictions and experiment in Figure 16 indicates that the commercial unit is performing well. In this way laboratory results from single tubes can be used as a benchmark for the performance of commercial units, serious underperformance indicating problems, for instance, with cross talk.

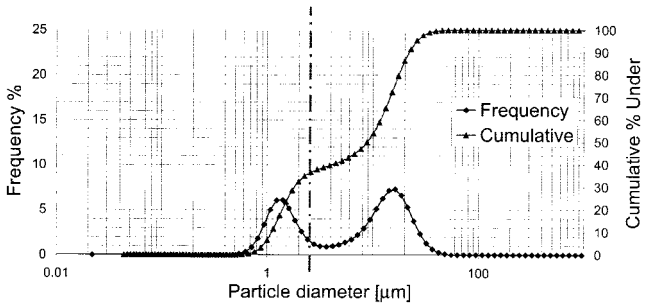

Figure 14. Particle-size distribution at the inlet to a commercial swirl-tube installation; the cut size predicted from the model swirl tube is indicated.

The GEC based on the laboratory model is slightly steeper than in the commercial unit, something that is often seen when comparing GECs from laboratory equipment with commercial units.

The size distribution of the feed to the commercial installation is shown in Figure 14. The size distribution is (due to the nature of the upstream gas cleaning equipment) bimodal with peaks at 1.3 and 15 μm. Based on the predicted and measured cut size of about 2.5 μm (see Figure 16; this size is also indicated in Figure 14), one would expect the peak to be removed by the TSS at larger sizes. This is also what is seen experimentally; the size distribution of the particles lost from the TSS is shown in Figure 15. This distribution is unimodal and the particles are very fine, the peak being close to the same position as the first peak in the feed.

The commercial value of the small x_{50} and the flatter shape of the GEC of the TSS is that:

(1) All particles larger than, say, 5 μm are fully separated, so that erosion of downstream turboexpanders is eliminated;

(2) Particles much smaller than x_{50} (e.g., the microfines $<$ 3 μm) are still separated, which reduces the chance of equipment fouling, which frequently is related to these microfines.

On the best modeling assumptions for swirl tubes

CFD and LDA results can be used to assess how well the flow assumptions in the two types of model mentioned in the Introduction reflect the real flow. The time-of-flight models have the following assumptions:

- The swirl velocity in the cyclone is constant axially;
- The velocity normal to the wall is negligible in the near-wall region, except in the bottom where a strong inwardly directed flow exists.

The equilibrium orbit models are concerned with the flow in the cylindrical surface CS obtained by prolonging the vortex-finder wall to the bottom. They assume:

- An axially constant swirl velocity in CS;
- A uniform radial velocity across CS.

LDA measurements (Peng et al., 2002) show that the tangential velocity in the swirl tube has a slight tendency to decrease as we move down the tube. Both CFD simulations and LDA measurements also indicate that little radial flow from the outer to the inner vortex takes place in the bulk of the separation space for swirl tubes, while this radial flow is more uniform axially in cylinder-on-cone cyclones. Hence, indica-

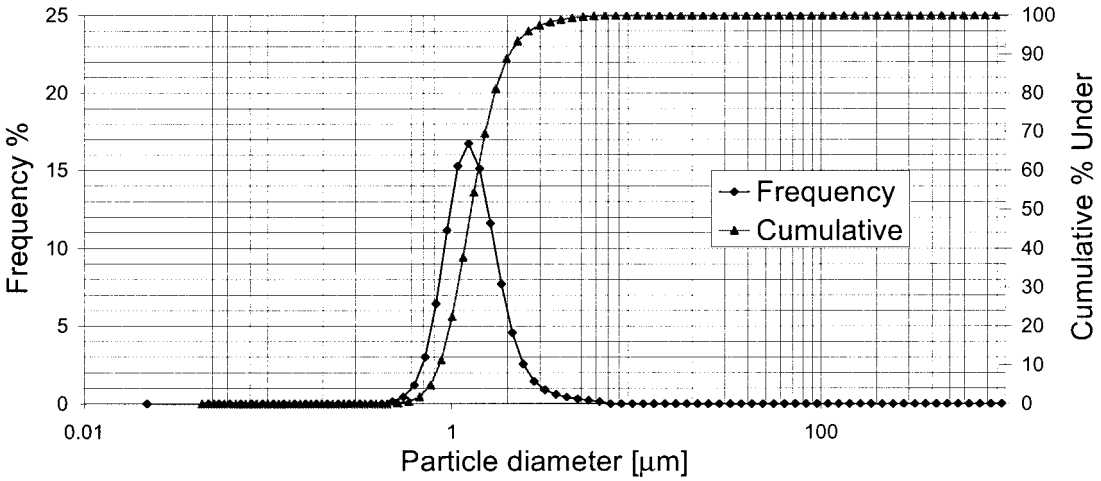

Figure 15. Particle-size distribution in the outlet from a well-performing commercial swirl-tube installation: the peak at the larger particle sizes has been removed as expected.

tions are that the equilibrium-orbit modeling concept is not as obviously appropriate in cylindrical swirl tubes as in cylinder-on-cone cyclones and that a swirl-tube model consistent with the physics of the process may better be based, at least in part, on some variant of the time-of-flight concept. A problem with this concept remains that the important effect of the vortex-finder diameter on the separation is difficult to account for.

Conclusions

(1) The performance of a swirl tube has been measured precisely under controlled laboratory conditions in a setup based on total capture of the overhead material stream.

(2) A *Stk-Eu* analysis shows that the overall performance of the swirl tube is as good as a "well-designed cyclone" in spite of the simpler body shape.

(3) Direct comparison using the scaling rules and simple models show that, of the two separators tested, the swirl tube is the more compact when operated at otherwise similar values for the performance parameters.

(4) The exponent m in Eq. 4 fitted to the GEC took on values in the 2.5–3.0 region in the swirl tube, while in the cylinder-on-cone cyclone it was 4.0. The swirl-tube GEC shape is therefore flatter, but the value of m is still well within the range of industrial cylinder-on-cone cyclones. In spite of the flatter shape around the cut size, the ranges of particles completely separated in swirl tubes and cylinder-on-cone, tangential-inlet cyclones are similar when the cut sizes are similar.

(5) The GEC predicted for a commercial FCC third-stage separator (TSS) on the basis of the laboratory model results matched the experimental results for the TSS well. Such scaled laboratory-model data can serve as a useful benchmark for industrial units, indicating the best possible separation with the given swirl-tube design. Performance degradation due to cross talk was seen to be absent in this case.

(6) Some variant of the time-of-flight modeling concept appears to be more consistent with the flow in swirl tubes than the equilibrium orbit concept.

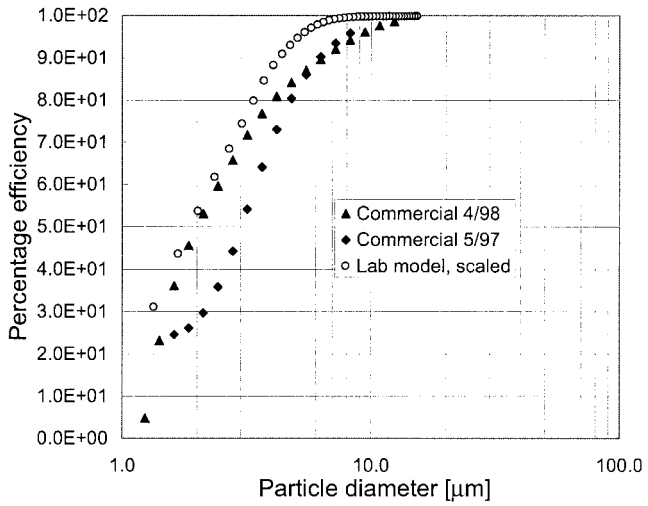

Figure 16. Experimental GECs from commercial swirl-tube installations (solid points) and predictions from the laboratory tube (open circles).

Acknowledgments

The authors acknowledge funding from the Norwegian Research Council during the preparation of this paper. They also thank the students and researchers carrying out the experiments and CFD simulations presented here: J. Kater (Shell) and R. S. Postma, A. Udding, M. de Groot and A. Berrino (University of Groningen).

Notation

c = constant
C_{y50} = a "characteristic cyclone number" determined empirically
D, D_a, D_b = cyclone (swirl-tube) body diameter.
D_x = vortex finder diameter
Eu = Euler number = $\Delta p/(\frac{1}{2}\,\rho v^2)$
F = horizontal, cross-sectional area of the vanes outlet section
$F_f(x)$, $F_c(x)$, $F(x)$ = cumulative size distributions of the fines (lost), the captured, and the feed material fractions, respectively
H = overall height of the cyclone

$H_{25/75}$ = a measure of the slope of the GEC indicating the "sharpness of cut"
L_2 = distance between the gas outlet lip and the collection-chamber top
m = exponent in Eq. 4
N_s = the number of spiral turns the particle takes on its way toward the bottom of the cyclone
P = cyclone pressure drop
Q = volumetric gas flow rate
R_o = radius of the interface between the inner and outer vortice
R_w = radius of cyclone (swirl-tube) body = $D/2$
Stk_{50} = Stokes number for the cut size = $\Delta\rho x_{50}^2\langle v_z\rangle/18\mu D$
Stk_η = Stokes number for the particle size separated with an efficiency of η
v_{in} = inlet velocity
v_{rCS}, $v_{\theta CS}$ = radial and tangential velocity at the interface between the inner and outer vortice
v_θ = swirl velocity in cyclone (swirl tube)
$v_{\theta w}$ = swirl velocity at the cyclone wall
v_z = mean axial velocity = $Q/(\pi D^2/4)$
x = particle size (diameter)
x_{50} = cut size

Greek letters

θ = the exit angle of the vanes along the circumference direction
ρ_p, ρ = densities of particle and gas, $\Delta\rho = \rho_p - \rho$
η_T = total separation efficiency
$\eta(x)$ = fractional separation efficiency for size x [grade-efficiency curve (GEC)]
μ = gas viscosity

Literature Cited

Barth, W., "Berechnung und Auslegung von Zyklonabscheidern auf Grund neuerer Unterscuhungen," *Brennstoff-Wärme-Kraft,* **8**(1), 1 (1956).

Behrouzi, P., "Performance of Multicell, Axial-Entry Cyclones for Industrial Gas Cleaning," PhD Thesis, Dept. of Mechanical Engineering, Imperial College, Univ. of London (1988).

Clift, R., M. Ghadiri, and A. C. Hoffmann, "A Critique of Two Models for Cyclone Performance," *AIChE J.,* **37,** 285 (1991).

Dietz, P. W., "Collection Efficiency of Cyclone Separators," *AIChE J.,* **27,** 888 (1981).

Dirgo, J., and D. Leith, "Performance of Theoretically Optimised Cyclones," *Filtration Sep.,* **22,** 119 (1985).

Dries, H., and M. Patel, "New Advances in Third Stage Separators," *World Refining,* Oct. issue, p. 30 (2000).

Hoekstra, A. J., J. J. Derksen, and H. E. A. Van den Akker, "A CFD Study on the Performance of a High-Efficiency Gas Cyclone," *Proc. Int. Symp. on Computational Technologies for Fluid/Thermal/Structural/Chemical Systems with Industrial Applications,* Vol. 397-2, ASME-PVP, Fairfield, NJ, p. 219 (1999).

Hoffmann, A. C., M. de Groot, W. Peng, H. W. A. Dries, and J. Kater, "Advantages and Risks in Increasing Cyclone Separator Length," *AIChE J.,* **47,** 2452 (2001).

Hoffmann, A. C., and L. E. Stein, *Gas Cyclones and Swirl Tubes—Principles, Design and Operation,* Springer-Verlag, Berlin (2002).

Mothes, H., and F. Löffler, "Prediction of Particle Removal in Cyclone Separators," *Int. Chem. Eng.,* **28,** 231 (1988).

Peng, W., A. C. Hoffmann, P. Boot, A. Udding, H. W. A. Dries, A. Ekker, and J. Kater, "Flowpattern in Reverse-Flow Centrifugal Separators," *Powder Technol.,* **127,** 212 (2002).

Rietema, K., "The Mechanism of Separation of Finely Dispersed Solids in Cyclones," *Proc. Symp. Cyclones,* Utrecht, The Netherlands, p. 46 (1958).

Rosin, P., E. Rammler, and W. Intelmann, "Grundlagen und Grenzen der zyklonentstaubung," *Zeit,* **76,** 433 (1932).

Svarovsky, L., "Solid-Gas Separation," *Gas Fluidization Technology,* D. Geldart, ed., Wiley, New York (1986).

Trefz, M., "Die verschiedenen Abscheidevorgänge im hoher und hoch beladenen Gaszyklon unter Besonderer Berücksichtigung der Serkundarströmung" (in German), Forschritt-Berichte VDI 295, VDI-Verlag GmbH, Düsseldorf.

Manuscript received Jan. 25, 2003, revision received May 25, 2003, and final revision received July 18, 2003.